A NON-OSCILLATORY SHOCK CAPTURING SCHEME USING FLUX LIMITED DISSIPATION

By

Antony Jameson
Princeton University

MAE Report #1653
April 1984

Lectures in Applied Mathematics, Vol. 22,
Large Scale Computations in Fluid Mechanics,
Edited by B. E. Engquist, S. Osher and R. C. J. Somerville

A.M.S., 1985
pp. 345-370

Note

I was not able to attend the meeting at La Jolla. Since I was invited to contribute a paper, however, I am offering the present work as a substitute for my presence. It contains an attempt to unify concepts stemming from the mathematical theory of shock waves with techniques which I have found to work well in practice.

I. Introduction

During the last decade computational methods in fluid dynamics have penetrated a variety of fields including airplane design, car design, ship design, studies of blood flow, oil recovery, oceanography, meteorology and astrophysics. Improvements in high speed electronic computers have made it feasible to attempt numerical calculations of progressively more complicated mathematical models of fluid flow.

Despite the intensive efforts of numerous investigators, the objective of combining

1) High accuracy

2) Resolution of shock waves and contact discontinuities

3) Elimination of spurious oscillations

continues to be an elusive goal. It has long been recognized that upwind differencing can eliminate spurious oscillations in the neighborhood of shock waves at the expense of low accuracy in regions where the flow is smooth. Central difference schemes, on the other hand, produce good solutions in smooth regions, but are prone to oscillations in the neighborhood of shock waves. These oscillations can be suppressed only by the introduction of additional dissipative terms.

Stemming from the mathematical theory of scalar conservation laws [1], Harten has recently proposed the concept of total variation diminishing (TVD)

difference schemes [2]. Harten also devised a second order accurate TVD scheme which incorporates flux limiters to control the action of an anti-diffusive term. Van Leer had earlier used flux limiters to produce a second order accurate scheme which would preserve the monotonicity of an initially monotone profile [3]. Important contributions to the theory of upwind schemes have also been made by Roe [4,5], and Osher [6,7]. Both have devised second order accurate upwind schemes using flux limiters. Many of the ideas on flux limiters have recently been unified by Sweby [8].

In parallel with these developments it has been found that steady aerodynamic flows containing moderately strong shock waves can be quite well predicted by a central difference scheme augmented by a carefully controlled blend of first and third order dissipative terms [9-11]. The third order terms provide background damping of high frequency modes. The first order terms are needed to control oscillations in the neighborhood of shock waves, and are turned on by sensing strong pressure gradients in the flow. Since the primary requirement has been the calculation of steady flows, it has proved convenient to separate the space and time discretization procedures. A semi-discrete model for a complex geometric domain is obtained by a subdivision into quadrilateral cells, and the resulting system of ordinary differential equations is then solved by a multi-stage time stepping procedure. Convergence to a steady state can be dramatically accelerated by using multiple grids [12-14], with the result that a transonic flow past an airfoil can be calculated in 25-50 steps.

My purpose in this paper is to suggest a method of modifying the third order dissipative terms by the introduction of flux limiters. The first order

dissipative terms can then be eliminated entirely, and in the case of a scalar conservation law, the scheme is converted into a total variation diminishing scheme provided that an appropriate value is chosen for the dissipative coefficient. The treatment of a scalar conservation law is discussed in the next Section. Section 3 reviews the application of these ideas to the treatment of the Euler equations for inviscid compressible flow, using a finite volume formulation to allow for a complex geometric domain. Section 4 reviews the boundary conditions, and Section 5 and 6 review the multi-stage time stepping and multigrid schemes. Finally Section 7 presents some preliminary results for transonic flows.

2. TVD Scheme for a Scalar Conservation Law

Consider the scalar conservation law

$$\frac{\partial u}{\partial t} + \frac{\partial}{\partial x} f(u) = 0 \tag{2.1}$$

It is well known that the total variation

$$TV = \int_{-\infty}^{\infty} \left|\frac{\partial u}{\partial x}\right| dx$$

cannot increase. Suppose now that a multi-point semi-discrete approximation to equation (2.1) is expressed in the form

$$\frac{du_i}{dt} = \sum_{q=-Q}^{Q-1} c_q(i)(u_{i-q} - u_{i-q-1}) \tag{2.2}$$

The discrete total variation is

$$TV = \sum_{i=-\infty}^{\infty} |u_i - u_{i-1}|$$

It can be shown [15] that this will not increase if and only if

$$c_{-1}(i-1) \geq c_{-2}(i-2) \ldots \geq c_{-Q}(i-Q) \geq 0 \tag{2.3a}$$

and

$$-c_0(i) \geq -c_1(i+1) \ldots \geq -c_{Q-1}(i+Q-1) \geq 0 \tag{2.3b}$$

Now consider the scheme

$$\frac{du_i}{dt} + \frac{1}{\Delta x}(h_{i+1/2} - h_{i-1/2}) = 0 \tag{2.4}$$

where $h_{i+1/2}$ is an approximation to the flux across the boundary between

the $(i+1)^{st}$ and i^{th} cells. Denoting $f(u_i)$ by f_i, define the numerical flux as

$$h_{i+1/2} = \frac{1}{2}(f_{i+1} + f_i) + d_{i+1/2} \tag{2.5}$$

where $d_{i+1/2}$ is a dissipative flux. Suppose that this is a constructed as

$$d_{i+1/2} = e_{i+3/2} - 2e_{i+1/2} + e_{i-1/2} \tag{2.6}$$

where

$$e_{i+1/2} = \alpha_{i+1/2}(u_{i+1} - u_i) \tag{2.7}$$

and $\alpha_{i+1/2}$ is a positive coefficient. According to equations (2.6) and (2.7) the dissipative flux is a quantity of third order. Now define

$$a_{i+1/2} = \begin{cases} \dfrac{f_{i+1} - f_i}{u_{i+1} - u_i} & \text{if } u_{i+1} \neq u_i \\ \left.\dfrac{\partial f}{\partial u}\right|_{u = u_i} & \text{if } u_{i+1} = u_i \end{cases}$$

and

$$\Delta_{i+1/2} = u_{i+1} - u_i$$

Then equation (2.4) becomes

$$\Delta x \frac{du_i}{dt} = -\frac{1}{2} a_{i+1/2} \Delta_{i+1/2} - \frac{1}{2} a_{i-1/2} \Delta_{i-1/2}$$

$$- \alpha_{i+3/2} \Delta_{i+3/2} + 3\alpha_{i+1/2} \Delta_{i+1/2} - 3\alpha_{i-1/2} \Delta_{i-1/2} + \alpha_{i-3/2} \Delta_{i-3/2}$$

This does not satisfy condition (2.3) because the coefficients of $\Delta_{i+3/2}$ and $\Delta_{i-3/2}$ have the wrong sign. In order to correct this we can modify the dissipa-

tive terms by the introduction of flux limiters. Denote the ratio of successive increments by

$$r_i = \frac{e_{i-1/2}}{e_{i+1/2}} \tag{2.8}$$

and define the function

$$\phi(r) = \begin{cases} 0, & r < 0 \\ r, & 0 \leq r \leq 1 \\ 1, & r > 1 \end{cases} \tag{2.9}$$

Also let

$$\psi(r) = \phi(\frac{1}{r}) \tag{2.10}$$

Since ϕ satisfies the symmetry condition

$$r\ \phi(\frac{1}{r}) = \phi(r)$$

it follows that

$$r\ \psi(r) = \phi(r) \leq 1$$

Denoting $\phi(r_i)$ by ϕ_i and $\psi(r_i)$ by ψ_i the dissipative flux is now redefined as

$$d_{i+1/2} = \phi_{i+1}\ e_{i+3/2} - 2e_{i+1/2} + \psi_i\ e_{i-1/2} \tag{2.11}$$

According to equation (2.8)

$$e_{i+3/2} = \frac{e_{i+1/2}}{r_{i+1}}\ ,\ e_{i-3/2} = r_{i-1}\ e_{i-1/2}$$

Therefore equation (2.4) now yields

$$\Delta x \frac{du_i}{dt} = -\frac{1}{2} a_{i+1/2} \Delta_{i+1/2} - \frac{1}{2} a_{i-1/2} \Delta_{i-1/2}$$

$$+ \left(2 - \frac{\phi_{i+1}}{r_{i+1}} + \phi_i\right) \alpha_{i+1/2} \Delta_{i+1/2}$$

$$- \left(2 - r_{i-1} \psi_{i-1} + \psi_i\right) \alpha_{i-1/2} \Delta_{i-1/2}$$

Since

$$0 \leqslant \phi(r) \leqslant 1 \quad , \quad 0 \leqslant \frac{\phi(r)}{r} \leqslant 1$$

and

$$0 \leqslant \psi(r) \leqslant 1 \quad , \quad 0 \leqslant r\,\psi(r) \leqslant 1$$

it follows that conditions (2.3) are satisfied if

$$\alpha_{i+1/2} \geqslant \frac{1}{2} |a_{i+1/2}| \quad , \quad \alpha_{i-1/2} \geqslant \frac{1}{2} |a_{i-1/2}|$$

In a region where the solution is smooth

$$r_i = 1 + 0(\Delta x)$$

with the result that

$$\phi_i = 1 + 0(\Delta x) \ , \ \psi_i = 1 + 0(\Delta x)$$

and the modification of equation (2.6) is of second order.

A convenient alternative expression for the dissipative flux is obtained by introducing Roe's min mod function [8]. This can be defined as

$$B(p,q) = (s(p) + s(q)) \min (|p|, |q|)$$

where

$$s(p) = \begin{cases} \frac{1}{2} & \text{if } p \geq 0 \\ \frac{-1}{2} & \text{if } p < 0 \end{cases}$$

Then the dissipative flux (2.11) becomes

$$d_{i+1/2} = B(e_{i+3/2}, e_{i+1/2}) - 2e_{i+1/2} + B(e_{i+1/2}, e_{i-1/2})$$

One could also use a flux limiting function $\phi(r)$ satisfying a less stringent condition

$$0 \leq \phi(r) \leq K \ , \quad 0 \leq \frac{\phi(r)}{r} \leq K$$

where $K < 2$. Then one needs

$$\alpha_{i+1/2} \geq \frac{1}{2(2-K)} \ |a_{i+1/2}|$$

3. Finite volume scheme for the Euler Equations

Let p, ρ, u, v, E, H and c denote the pressure, density, Cartesian velocity components, total energy, total enthalpy and speed of sound. For a perfect gas

$$E = \frac{p}{(\gamma-1)\rho} + \frac{1}{2}(u^2 + v^2), \quad H = E + \frac{p}{\rho} \tag{3.1}$$

and

$$c^2 = \frac{\gamma p}{\rho}$$

where γ is the ratio of specific heats. Consider a domain S with boundary ∂S. The Euler equations for two-dimensional compressible flow can be written in integral form as

$$\frac{\partial}{\partial t} \iint_S w\,dS + \int_{\partial S} (f\,dy - g\,dx) = 0 \tag{3.2}$$

where x and y are Cartesian coordinates, t is the time coordinate, and

$$w = \begin{bmatrix} \rho \\ \rho u \\ \rho v \\ \rho E \end{bmatrix}, \quad f = \begin{bmatrix} \rho u \\ \rho u^2 + p \\ \rho uv \\ \rho uH \end{bmatrix}, \quad g = \begin{bmatrix} \rho v \\ \rho vu \\ \rho v^2 + p \\ \rho vH \end{bmatrix} \tag{3.3}$$

These equations are to be solved for a steady state $\frac{\partial w}{\partial t} = 0$.

In order to derive a semi-discrete model which can be used to treat complex geometric domains, the computational domain is divided into quadrilateral cells labelled by the subscripts i, j, as illustrated in Figure 1. Assuming that the dependent variables are known at the center of each cell, a system of ordinary differential equations is obtained by applying equation (3.2) separately to each cell. These have the form

$$\frac{d}{dt}\,(S_{i,j}\ w_{i,j}) + Q_{i,j} = 0 \tag{3.4}$$

where $S_{i,j}$ is the cell area, and $Q_{i,j}$ is the net flux out of the cell. This can be evaluated as

$$\sum_{k=1}^{4}\ (\Delta y_k\ f_k - \Delta x_k\ g_k) \tag{3.5}$$

where f_k and g_k denote values of the flux vectors f and g on the kth edge, Δx_k and Δy_k are the increments of x and y along the edge with appropriate signs, and the sum is over the four sides of the cell. The flux vectors are evaluated by taking the average of the values in the cells on either side of each edge. For example

$$f_2 = \frac{1}{2}\,(f_{i+1,j} + f_{i,j}) \tag{3.6}$$

where $f_{i,j}$ denotes $f(w_{i,j})$. This scheme reduces to a central difference scheme on a Cartesian grid, and is second order accurate if the mesh is sufficiently smooth. It also has the property that uniform flow is an exact solution of the difference equations.

The scheme as it stands is not resistant to high frequency oscillations between odd and even mesh points. Dissipative terms must be added to suppress spurious oscillations of this type, and to prevent the appearance of unsightly wiggles in the neighborhood of shock waves. With the addition of dissipative terms $D_{i,j}$, the semi-discrete equations (3.2) take the form

$$\frac{d}{dt}(S_{i,j}\ w_{i,j}) + Q_{i,j} - D_{i,j} = 0 \tag{3.7}$$

The dissipative terms can be introduced by augmenting the convective flux defined by equations (3.5-3.6) with a dissipative flux across each edge.

The convective flux across edge 2 in Figure 1 is

$$\frac{\Delta y}{2}(f_{i+1,j} + f_{i,j}) - \frac{\Delta x}{2}(g_{i+1,j} + g_{i,j})$$

Following Roe [4], one can introduce a matrix

$$C_{i+1/2,j} = C(w_{i+1,j}, w_{i,j})$$

with the property that

$$C_{i+1/2,j}(w_{i+1,j} - w_{i,j}) = \Delta y(f_{i+1,j} - f_{i,j}) - \Delta x(g_{i+1,j} - g_{i,j})$$

Thus C corresponds to the Jacobian matrix

$$\Delta y \frac{\partial f}{\partial w} - \Delta x \frac{\partial g}{\partial w}$$

Also $C_{i+1/2,j}$ can be expressed as

$$C_{i+1/2,j} = T \Lambda T^{-1}$$

where T is a matrix containing the eigenvectors of C as its columns, and Λ is a diagonal matrix containing the eigenvalues of C. The dissipative flux can now be constructed according to equation (2.11) by substituting each component of $T^{-1}(w_{i+1,j} - w_{i,j})$ in turn for $u_{i+1} - u_i$ in equation (2.7). The flux limiters are similarly defined in terms of ratios of these components between neighboring edges, while the dissipative coefficient $\alpha_{i+1/2}$ should be proportional to the magnitude of the corresponding eigenvalue.

An alternative approach is to bypass the characteristic decomposition and add dissipative terms directly constructed from the dependent variables. The dissipative flux for the density equation, for example, is constructed as

$$d_{i+1/2,j} = \phi_{i+1,j}\, e_{i+3/2} - 2e_{i+1/2} + \psi_{i,j}\, e_{i-1/2,j} \tag{3.8}$$

where

$$e_{i+1/2,j} = \alpha_{i+1/2,j}(\rho_{i+1,j} - \rho_{i,j}) \tag{3.9}$$

and $\alpha_{i+1/2,j}$ is a positive coefficient. The flux limiters are formed by taking

$$\phi_{i,j} = \phi(r_{i,j}), \qquad \psi_{i,j} = \psi(r_{i,j}) \tag{3.10}$$

where

$$r_{i,j} = \frac{e_{i-1/2,j}}{e_{i+1/2,j}} \tag{3.11}$$

and ϕ and ψ are defined by equations (2.9) and (2.10).

The dissipative fluxes for the momentum and energy equations are constructed in the same way as those for the mass equation, substituting ρu, ρv or ρH in equation (3.9). The purpose of using differences of ρH rather than ρE in the dissipative terms for the energy equation is to produce difference equations which admit a steady solution with constant total enthalpy. With this choice the energy equation reduces to the mass equation multiplied by a constant value of the total enthalpy when the time derivatives vanish.

The scheme corresponds to replacing the diagonal matrix Λ in the previous scheme by the identity matrix multiplied by the spectral radius of C. Thus if the dissipative coefficient $\alpha_{i+1/2}$ is set equal to one-half the spectral radius of C one can expect the scheme to suppress spurious oscillations. The spectral radius can be estimated as the value of

$$R = |\Delta y u - \Delta x v| + c\sqrt{\Delta x 2 + \Delta y 2}$$

on the edge separating cells i+1,j and i, j.

In practice this leads to an excessively dissipative scheme. This can be remedied by using an adaptive coefficient $\alpha_{i+1/2,j}$. For this purpose a sensor is introduced. A suitable choice is based on the second difference of the pressure

$$\nu_{i,j} = \left| \frac{p_{i+1,j} - 2p_{i,j} + p_{i-1,j}}{p_{i+1,j} + 2p_{i,j} + p_{i-1,j}} \right| \tag{3.12}$$

Then define

$$\bar{\nu}_{i+1/2,j} = \max (\nu_{i+2,j}, \nu_{i+1,j}, \nu_{i,j}, \nu_{i-1,j}) \tag{3.13}$$

and

$$\alpha_{i+1/2,j} = \min (\tfrac{1}{2}, k_0 + k_1 \bar{\nu}_{i+1/2,j}) \tag{3.14}$$

where the constant k_0 determines a threshold, and the constant k_1 is chosen to make sure that there is enough dissipation to suppress oscillations in the neighborhood of shock waves.

4. Boundary Conditions

At a solid boundary the only contribution to the flux balance (3.4) comes from the pressure. The normal pressure gradient $\frac{\partial p}{\partial n}$ at the wall can be estimated from the condition that $\frac{\partial}{\partial t}(\rho q_n) = 0$, where q_n is the normal velocity component. The pressure at the wall is then estimated by extrapolation from the pressure at the adjacent cell centers, using the known value of $\frac{\partial p}{\partial n}$.

The rate of convergence to a steady state will be impaired if outgoing waves are reflected back into the flow from the outer boundaries. The treatment of the far field boundary condition is based on the introduction of Riemann invariants for a one dimensional flow normal to the boundary. Let subscripts ∞ and e denote free stream values and values extrapolated from the interior cells adjacent to the boundary, and let q_n and c be the velocity component normal to the boundary and the speed of sound. Assuming that the flow is subsonic at infinity, we introduce fixed and extrapolated Riemann invariants

$$R_\infty = q_{n\infty} - \frac{2c_\infty}{\gamma-1}$$

and

$$R_e = q_{n_e} + \frac{2c_e}{\gamma-1}$$

corresponding to incoming and outgoing waves. These may be added and subtracted to give

$$q_n = \frac{1}{2}(R_e + R_\infty)$$

and

$$c = \frac{\gamma-1}{4}(R_e - R_\infty)$$

where q_n and c are the actual normal velocity component and speed of sound to be specified in the far field. At an outflow boundary, the tangential velocity

component and entropy are extrapolated from the interior, while at an inflow boundary they are specified as having free stream values. These four quantities provide a complete definition of the flow in the far field. If the flow is supersonic in the far field, all the flow quantities are specified at an inflow boundary, and they are all extrapolated from the interior at an outflow boundary.

5. Multi-stage Time stepping Schemes

Since the cell area $S_{i,j}$ is independent of time, equation (3.7) can be written as

$$\frac{dw}{dt} + R(w) = 0 \tag{5.1}$$

where R(w) is the residual

$$R_{ij} = \frac{1}{S_{i,j}} (Q_{i,j} - D_{i,j}) \tag{5.2}$$

Here Q(w) is the convective operator defined by equations (3.5-3.6) and D(w) is the dissipative operator, defined, for example, by equations (3.8-3.9)

Equation (5.1) is now to be integrated to reach a steady state as rapidly as possible. Multi-stage time stepping schemes prove to be effective for this purpose, and they can also readily be adapted to drive a multigrid procedure. The TVD property which is obtained by the construction of Section 2 for a semi-discrete scheme can also be established for an explicit time stepping scheme, provided that a restriction is imposed on the time step [15]. In the present application, however, spurious oscillations could be tolerated in the transient phase as long as they vanish in the steady state.

Multi-stage schemes for the numerical solution of ordinary differential equations are usually designed to give a high order of accuracy. Since the present objective is simply to obtain a steady state as rapidly as possible, the order of accuracy is not important. This allows the use of schemes selected purely for their properties of stability and damping. For this purpose it pays to distinguish the hyperbolic and parabolic parts stemming respectively from the convective and dissipative terms, and to treat them differently. This leads to a new class of hybrid multi-stage schemes.

Dropping the subscripts i,j the general m stage hybrid scheme to advance a time step Δt can be written as

$$\begin{aligned} w(0) &= w^n \\ w(1) &= w(0) - \alpha_1 \quad \Delta t \; R(0) \\ &\cdots \\ w(m-1) &= w(0) - \alpha_{m-1} \; \Delta t \; R^{(m-2)} \\ w(m) &= w(0) - \quad \Delta t \; R^{(m-1)} \\ w^{n+1} &= w(m) \end{aligned} \tag{5.3}$$

where w^n and w^{n+1} are the values at the beginning and end of the time step, and the residual in the q+1st stage is evaluated as

$$R^{(q)} = \frac{1}{S} \sum_{r=0}^{q} \{\beta_{qr} Q(w^{(r)}) - \gamma_{qr} D(w^{(r)})\} \tag{5.4}$$

subject to the consistency constraint that

$$\sum_{r=0}^{q} \beta_{qr} = \sum_{r=0}^{q} \gamma_{qr} = 1 \tag{5.5}$$

A useful insight into the behavior of these schemes can be gained by considering the model problem

$$u_t + u_x + \mu \Delta x^3 \; u_{xxxx} = 0 \tag{5.6}$$

In the absence of the third order dissipative term this equation describes the propagation of a disturbance without distortion at unit speed. With centered differences the residual has the form

$$\begin{aligned} \Delta t R_i = & \frac{\lambda}{2} (u_{i+1} - u_{i-1}) \\ & + \lambda\mu(u_{i+2} - 4u_{i+1} + 6u_i - 4u_{i-1} + u_{i-2}) \end{aligned}$$

where $\lambda = \Delta t/\Delta x$ is the Courant number. If we consider a Fourier mode $\hat{u} = e^{ipx}$

the discretization in space yields

$$\Delta t \ \frac{d\hat{u}}{dt} = z\hat{u}$$

where z is the Fourier symbol of the residual. Setting $\xi = p\Delta x$, this is

$$z = -\lambda i \sin\xi - 4\lambda\mu(1 - \cos\xi)^2 \tag{5.7}$$

In the complex plane z describes an oval path as ξ ranges from $-\pi$ to π. A single step of the multistage scheme yields

$$\hat{u}^{n+1} = g(z)\hat{u}^n$$

where g(z) is the amplification factor. The stability region of the scheme is given by those values of z for which $g(z) \leq 1$.

A simple procedure is to recalculate the residual at each stage using the most recently updated value of w. Then (5.4) becomes

$$R^{(q)} = \frac{1}{S}\left\{Q(w^{(q)}) - D(\overset{(q)}{w})\right\} \tag{5.8}$$

Schemes of this subclass have been analyzed in a book by van der Houwen [16], and more recently in papers by Sonneveld and van Leer [17], and Roe and Pike [18]. They are second order accurate in time for both linear and nonlinear problems if $\alpha_{m-1} = 1/2$. An efficient 4 stage scheme, which is also fourth order accurate for linear problems, has the coefficients

$$\alpha_1 = 1/4 \quad , \alpha_2 = 1/3 \quad , \alpha_3 = 1/2$$

The amplification factor of this scheme is given by the polynomial

$$g(z) = 1 + z + \frac{z^2}{2} + \frac{z^3}{6} + \frac{z^4}{24}$$

The stability region of this scheme is shown in Figure 2(a), which displays contour lines for $|g| = 1, .9, .8, \ldots$. The Figure also shows the locus of z as the wave number is varied between 0 and 2π for a Courant number $\lambda = 2.8$, and a dissipation coefficient $\mu = 1/32$. The corresponding variation of $|g|$ with ξ is shown in Figure 2(b). The intercept of the stability region with the imaginary axis is $2\sqrt{2}$; the corresponding bound on the time step is $\Delta t \leq 2\sqrt{2}\ \Delta x$.

The maximum stability interval along the imaginary axis attainable by an m stage scheme is m-1. This has been proved for the case when m is odd by van der Houwen, who also gave formulas for the coefficients α_q [16]. The case of m even has recently been solved by Sonneveld and van Leer [17]. For example, the 4 stage scheme with coefficients

$$\alpha_1 = 1/3 \quad , \alpha_2 = 4/15 \quad , \quad \alpha_3 = 5/9$$

has a stability region extending to 3 along the imaginary axis, at the expense of a slight reduction along the real axis.

The computational requirements of a multi-stage scheme can be substantially reduced by freezing the dissipative part of the residual at the value $D(w^{(0)})$ in all stages of the scheme, so that in the $(q+1)^{st}$ stage

$$R^{(q)} = \frac{1}{S}\left\{Q(w^{(q)}) - D(w^{(0)})\right\} \tag{5.9}$$

The amplification factor can no longer be represented as a polynomial, but it can easily be calculated recursively. If the time stepping scheme is to be used in a multi-grid procedure it is important that it should be effective at damping high frequency modes. One can fairly easily devise 3 and 4 stage schemes in the

class defined by (5.9) which meet this requirement. An effective 3 stage scheme is given by the coefficients

$$\alpha_1 = .6, \qquad \alpha_2 = .6 \quad .$$

Its stability region is shown in Figure 3.

Additional flexibility is provided by a class of schemes in which the dissipative terms are evaluated twice. This may be used to make a further improvement in the high frequency damping properties, or else to extend the stability region along the real axis to allow more margin for the dissipation introduced by a TVD scheme. In this class of schemes

$$R^{(0)} = \frac{1}{S}\left\{Q(w^{(0)}) - D(w^{(0)})\right\}$$

and

$$R^{(q)} = \frac{1}{S}\left\{Q(w^{(q)}) - \beta D(w^{(1)}) - (1-\beta)D(w^{(0)})\right\} \qquad , \; q \geq 1 \tag{5.10}$$

In the case of pure dissipation ($Qw = 0$), the amplification factor reduces to

$$g = 1 + z + \alpha_1\beta\, z^2$$

Thus if β is chosen such that $\alpha_1\beta = 1/4$, the stability region will contain a double zero at $z = -2$ on the real axis. A maximum stability interval of 8 can be attained along the real axis by choosing β such that $\alpha_1\beta = 1/8$. Figure 4 shows the stability region of a 5 stage scheme in this class with the coefficients

$$\alpha_1 = 1/4, \quad \alpha_2 = 1/6, \quad \alpha_3 = 3/8, \quad \alpha = 1/2, \quad \beta = 1 \tag{5.11}$$

This scheme combines van der Houwen's optimal coefficients with two evaluations of the dissipative terms to attain a stability interval of 4 along both the imaginary and the real axes.

As it stands the maximum permissable time step is restricted by the stability limit on the Courant number. This restriction can be relaxed by replacing the residual at each point by a weighted average of the neighboring residuals. In a one dimensional case one might replace the residual R_i by the average

$$\bar{R}_i = \varepsilon R_{i-1} + (1-2\varepsilon)\ R_i + \varepsilon R_{i+1}$$

at each stage of the scheme. This smooths the residuals and also increases the support of the scheme, thus relaxing the restriction on the time step imposed by the Courant Friedrichs Lewy condition. If $\varepsilon \geq 1/4$, however, there are Fourier modes such that $\bar{R}_i = 0$ when $R_i \neq 0$. To avoid this restriction it is better to perform the averaging implicitly by setting

$$-\varepsilon\bar{R}_{i-1} + (1 + 2\varepsilon)\ \bar{R}_i - \varepsilon\bar{R}_{i+1} = R_i \tag{5.12}$$

For an infinite interval this equation has the explicit solution

$$R_i = \frac{1-r}{1+r} \sum_{q=-\infty}^{\infty} r^q\ R_{i+q} \tag{5.13}$$

where

$$\varepsilon = \frac{r}{(1-r)^2} \quad , \ r < 1 \tag{5.14}$$

Thus the effect of the implicit smoothing is to collect information from residuals at all points in the field, with an influence coefficient which decays by factor r at each additional mesh interval from the point of interest.

Consider the model problem (5.6). According to equation (5.12) the Fourier symbol (5.7) will be replaced by

$$z = -\lambda \frac{i \sin \xi + 4\mu(1-\cos\xi)^2}{1 + 2\varepsilon(1-\cos\xi)}$$

In the absence of dissipation one now finds that stability can be maintained for any Courant number λ, provided that the smoothing parameter satisfies the condition

$$\varepsilon \geq \frac{1}{4} \left\{ \frac{\lambda^2}{\lambda^{*2}} - 1 \right\}$$

where λ^* is the stability limit of the unsmoothed scheme.

In the two dimensional case the implicit residual averaging is applied in product form

$$(1 - \varepsilon_x \delta_x^2)(1 - \varepsilon_y \delta_y^2) \bar{R} = R$$

where δ_x^2 and δ_y^2 are second difference operators in the x and y directions, and ε_x and ε_y are the corresponding smoothing parameters. In practice the best rate of convergence is usually obtained by using a value of λ about three times λ^*, and the smallest possible amount of smoothing to maintain stability.

6. Multigrid Scheme

While the available theorems in the theory of multigrid methods generally assume ellipticity, it seems that it ought to be possible to accelerate the evolution of a hyperbolic system to a steady state by using large time steps on coarse grids, so that disturbances will be more rapidly expelled through the outer boundary. The interpolation of corrections back to the fine grid will introduce errors, however, which cannot be rapidly expelled from the fine grid, and ought to be locally damped if a fast rate of convergence is to be attained. Thus it remains important that the driving scheme should have the property of rapidly damping out high frequency modes.

Ni [19] and Denton [20] have succeeded in accelerating convergence to a steady state by distributing the residuals from the fine grid to a series of coarser grids and calculating bulk corrections for the aggregated cells on the coarse grids. Both these schemes introduce first order dissipative terms. The flexibility in the formulation of the hybrid multi-stage time stepping schemes allows them to be matched with higher order dissipative terms to provide effective damping of the high frequency modes. This makes it possible to devise rapidly convergent multigrid schemes without any need to compromise the accuracy through the introduction of excessive levels of dissipation.

In order to adapt the multi-stage scheme for a multigrid algorithm , auxiliary meshes are introduced by doubling the mesh spacing. Values of the flow variables are transferred to a coarser grid by the rule

$$w_{2h}^{(0)} = (\sum S_h w_h)/S_{2h} \tag{6.1}$$

where the subscripts denote values of the mesh spacing parameter, S is the cell area, and the sum is over the 4 cells on the fine grid composing each cell on the coarse grid. This rule conserves mass, momentum and energy. A forcing function is then defined as

$$P_{2h} = \sum R_h(w_h) - R_{2h}(w_{2h}^{(0)}) \tag{6.2}$$

where R is the residual of the difference scheme. In order to update the solution on a coarse grid, the multistage scheme (4.3) is reformulated as

$$\begin{aligned} w^{(1)} &= w_{2h}^{(0)} - \alpha_1 \Delta t (R_{2h}^{(0)} + P_{2h}) \\ &\cdots \\ w_{2h}^{(q+1)} &= w_{2h}^{(0)} - \alpha_q \Delta t \, (R_{2h}^{(q)} + P_{2h}) \\ &\cdots \end{aligned} \tag{6.3}$$

where $R^{(q)}$ is the residual at the $q+1^{st}$ stage. In the first stage of the scheme, the addition of P_{2h} cancels $R_{2h}(w_{2h}^{(0)})$ and replaces it by $\sum R_h(w_h)$, with the result that the evolution on the coarse grid is driven by the residuals on the fine grid. This process is repeated on successively coarser grids. Finally the correction calculated on each grid is passed back to the next finer grid by bilinear interpolation.

Since the evolution on a coarse grid is driven by residuals collected from the next finer grid, the final solution on the fine grid is independent of the choice of boundary conditions on the coarse grids. The surface boundary condition is treated in the same way on every grid, by using the normal pressure gradient to extrapolate the surface pressure from the pressure in the cells adjacent to the wall. The far field conditions can either be transferred from the fine grid, or recalculated by the procedure described in Section 6.

It turns out than an effective multigrid strategy is to use a simple saw tooth cycle (as illustrated in Figure 5, in which a transfer is made from each grid to the next coarser grid after a single time step. After reaching the coarsest grid the corrections are then successively interpolated back from each grid to the next finer grid without any intermediate Euler calculations. On each grid the time step is varied locally to yield a fixed Courant number, and the same Courant number is generally used on all grids, so that progressively larger time steps are used after each transfer to a coarser grid. In comparison with a single time step of the Euler scheme on the fine grid, the total computational effort in one multigrid cycle is

$$1 + \frac{1}{4} + \frac{1}{16} + \ldots < \frac{4}{3}$$

plus the additional work of calculating the forcing functions P, and interpolating the corrections. The effective time step of a complete cycle using n grids is roughly

$$(1 + 2 + 4\ldots + 2^{n-1})\Delta t = (2^n - 1)\Delta t$$

where Δt is the time step on the fine grid.

7. Results

This section presents some preliminary results which have been obtained with a computer program incorporating the ideas presented in the previous sections. The dissipative terms were directly calculated from the dependent variables according to equations (3.8 - 3.14), without a decomposition into characteristic fields. The multigrid scheme was driven by the 5 stage time stepping scheme defined by equations (5.10 - 5.11), together with residual averaging. A variable time step corresponding to a fixed local Courant number of about 7.5 was used on all grids. An additional measure which was used to improve convergence was the introduction of forcing terms proportional to the difference between the local value of the total enthalpy and its free stream value [9]. The terms added to the mass and momentum equations are $\alpha\rho(H-H_\infty)$, $\alpha\rho u(H-H_\infty)$ and $\alpha\rho v(H-H_\infty)$, while that added to the energy equation is $\alpha\rho(H-H_\infty)$. The constant α is chosen empirically.

The first example is the transonic flow past an NACA 64A410 airfoil at Mach .720 and an angle of attack $\alpha = 0^o$. Figure 6(a) shows the inner part of the grid, which contained 160 cells in the circumferential direction and 32 cells in the direction normal to the profile. Figure 6(b) displays the final pressure distribution in terms of the pressure coefficient

$$c_p = (p - p_\infty)/1/2\ \rho_\infty\ q_\infty^2$$

There is a moderately strong shock wave at about 60% of the chord on the upper surface. This result was obtained with 25 multigrid cycles on an 40 x 8 mesh, followed by 25 cycles on an 80 x 16 mesh, and finally 25 cycles on the 160 x 32

mesh. 2 grid levels were used in the multigrid scheme on the 40 x 8 mesh, 3 grid leves on the 80 x 16 mesh, and 4 grid levels on the 160 x 32 mesh. Figure 6(c) shows the convergence history on the 160 x 32 mesh. Two measures are displayed. One curve shows the decay of the logarithm of the error (measured by the root mean square root of change of the density). The other curve shows the build up of the number of grid points in the supersonic zone, which is a useful measure of global convergence. It can be seen that this number is already fixed.

The second example is the flow past the well known NACA 0012 airfoil at Mach .800 and $\alpha = 1.25^{o}$. The result is shown in Figure 7. The flow exhibits a much stronger shock wave on the upper surface, and a very weak shock wave on the lower surface. These are both captured with a numerical shock structure containing three interior cells, with a barely visible tail.

8. Conclusion

The numerical results suggest that a central difference scheme augmented by flux limited dissipative terms can lead to an effective non-oscillatory shock capturing method. Schemes constructed in this manner do not require a characteristic decomposition to assure their stability. It should be possible, however, to sharpen the resolution of shock waves and contact discontinuities by using a characteristic decomposition to allow more precise tailoring of the dissipative terms. Further numerical experiments will be required to determine the trade-off between the improved resolution and the increased computational complexity.

Acknowledgement

This work has benefited from the support of both the Office of Naval Research, under Grant N00014-81-K-0379 and the NASA Langley Research Center, under Grant NAG-1-186.

References

1. Lax, P. D., "Hyperbolic Systems of Conservation Laws and the Mathematical Theory of Shock Waves", SIAM Regional Series on Applied Mathematics, 11, 1973.

2. Harten, A., "High Resolution Schemes for Hyperbolic Conservation Laws", New York University Report DOE/ER 03077-175, 1982.

3. van Leer, B., "Towards the Ultimate Conservative Difference Scheme. II Monotonicity and Conservation Combined in a Second Order Scheme," J. Computational Physics, 14, 1974, pp. 361-370.

4. Roe, P. L., "The Use of the Riemann Problem in Finite Difference Schemes", Proc. 7th International Conference on Numerical Methods in Fluid Dynamics, Stanford 1980, edited by W. C. Reynolds and R. W. MacCormack, Springer, 1981, pp. 354-359.

5. Roe, P. L., "Approximate Riemann Solvers, Parameter Vectors, and Difference Schemes", J. Computational Physics, 43, 1981, pp. 357-372.

6. Osher, Stanley, "Riemann Solvers, The Entropy Condition, and Difference Approximations", To appear in SIAM Journal on Numerical Analysis.

7. Osher, S. and Chakravarthy, Sukumar, "High Resolution Schemes and the Entropy Condition", ICASE Report NASA CR 172218.

8. Sweby, P. K., "High Resolution Schemes Using Flux Limiters for Hyperbolic Conservation Laws", to appear in J. Computational Physics.

9. Jameson, Antony, "Transonic Aerofoil Calculations Using the Euler Equations", Proc. IMA Conference on Numerical Methods in Aeronautical Fluid Dynamics, Reading, 1981, edited by P. L. Roe, Academic Press, 1982, pp. 289-308.

10. Jameson, A., Schmidt, W., and Turkel, E., "Numerical Solution of the Euler Equations by Finite Volume Methods Using Runge-Kutta Time Stepping Schemes", AIAA Paper 81-1259, 1981.

11. Jameson, Antony, and Baker, Timothy J., "Solution of the Euler Equations for Complex Configurations", Proc. AIAA 6th Computational Fluid Dynamics Conference, Danvers, 1983, pp. 293-302.

12. Jameson, Antony, "Solution of the Euler Equations by a Multigrid Method", Applied Mathematics and Computation, 13, 1983, pp. 327-356.

13. Jameson, Antony, and Baker, T.J., "Multigrid Solution of the Euler Equations for Aircraft Configurations", AIAA Paper 84-0093, 1984.

14. Baker, T. J., Jameson, A., and Schmidt, W., "A Family of Fast and Robust Euler Codes", Proc. of Workshop on Computational Fluid Dynamics, Tullahoma, 1984, pp. 17.1-17.38.

15. Jameson, Antony, and Lax, Peter, D., "Conditions for the Construction of Multi-Point Total Variation Diminishing Difference Schemes", Princeton University Report MAE 1650, 1984.

16. P.J. Vander Houwen, "Construction of Integration Formulas for Initial Value Problems", North Holland, 1977.

17. Sonneveld, P., and van Leer, B., "Towards the Solution of Van der Houwen's Problems". To appear in Nieuw Archief voor Wiskunde.

18. Roe, P. L., and Pike, J., "Restructuring Jameson's Finite Volume Scheme for the Euler Equations", RAE Report, 1983.

19. Ni, R.H., "A Multiple Grid Scheme for Solving The Euler Equations", Proc. AIAA 5th Computational Fluid Dynamics Conference, Palo Alto, 1981, pp. 257-264.

20. Denton, J.D., "An Improved Time Marching Method for Turbomachinery Flow Calculation", Proc. IMA Conference on Numerical Methods in Aeronautical Fluid Dynamics, Reading, 1981, edited by P. L. Roe, Academic Press, 1982, pp. 189-210.

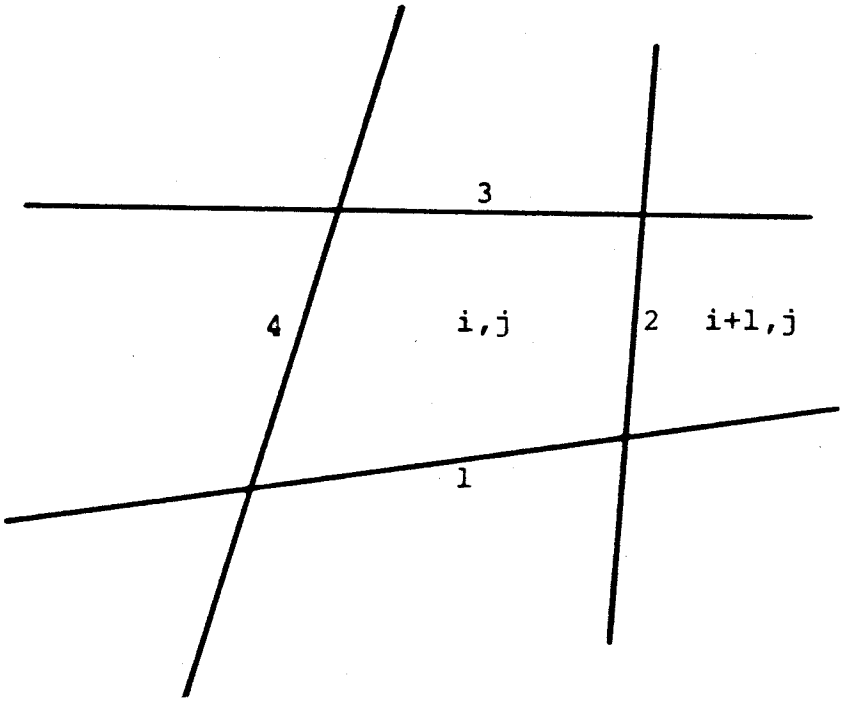

Figure 1

Finite Volume Scheme

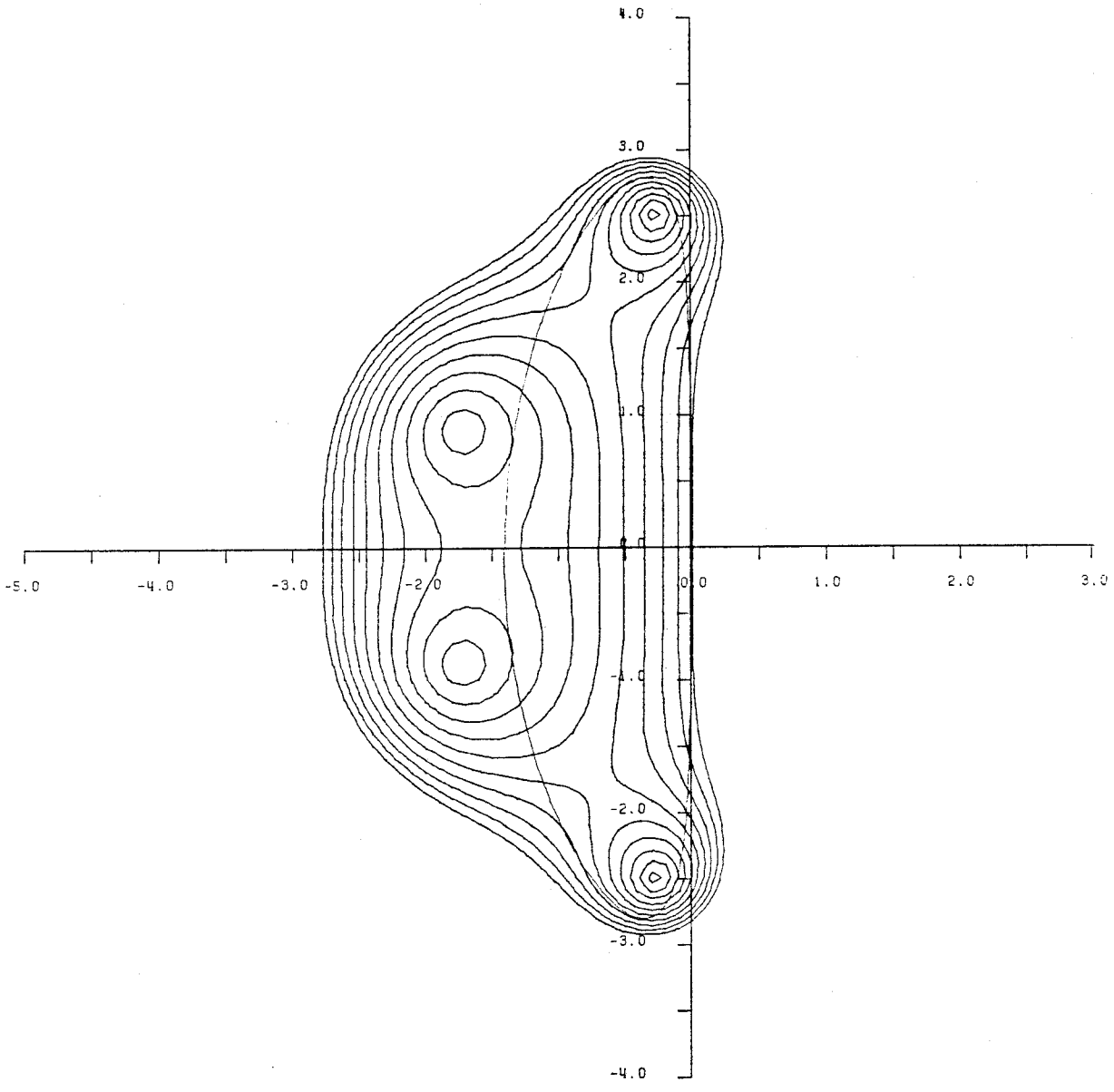

Figure 2(a)

Stability region of standard 4 stage scheme
Contour lines $|g| = 1., .9, .8, \ldots$
and locus of $z(\xi)$ for $\lambda = 2.8$, $\mu = 1/32$
Coefficients $\alpha_1 = 1/4$, $\alpha_2 = 1/3$, $\alpha_3 = 1/2$

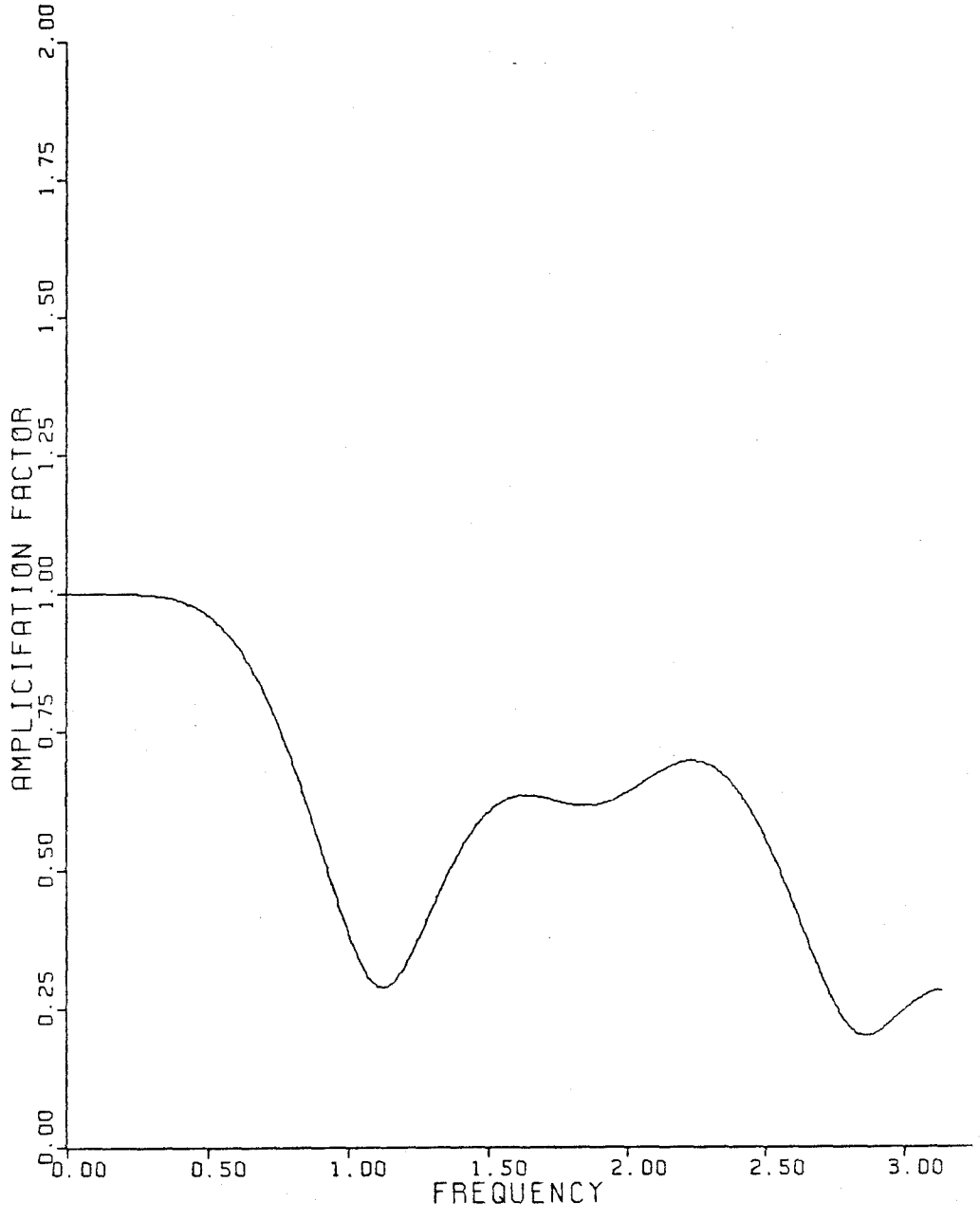

Figure 2(b)

Amplification factor $|g|$ of standard 4 stage scheme
for $\lambda = 2.8$, $\mu = 1/32$
Coefficients $\alpha_1 = 1/4$, $\alpha_2 = 1/3$, $\alpha_3 = 1/2$

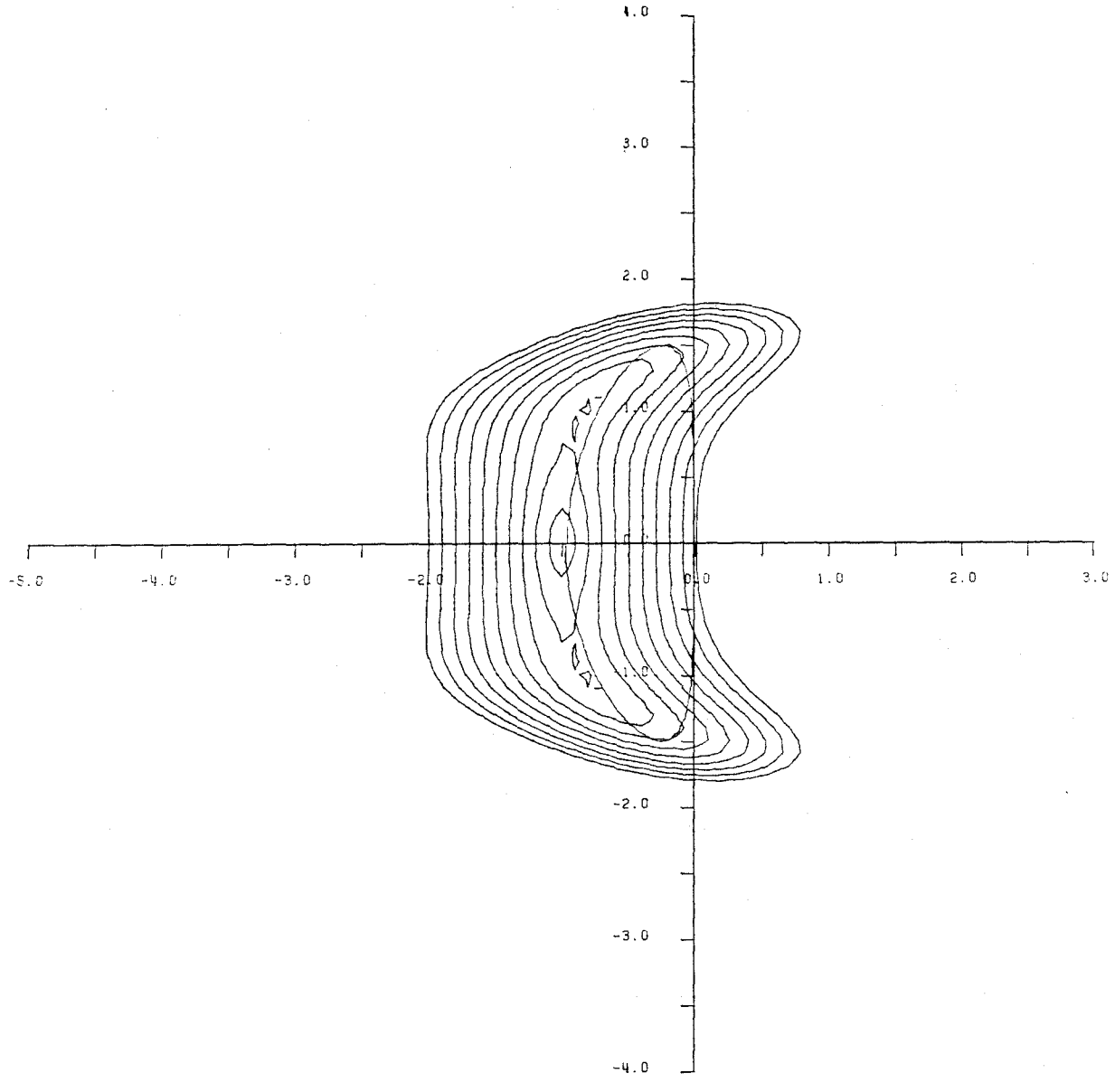

Figure 3(a)

Stability region of 3 stage scheme with single evaluation of dissipation
Contour lines $|g| = 1., .9, .8, \ldots$
and locus of $z(\xi)$ for $\lambda = 1.5$, $\mu = .04$
Coefficients $\alpha_1 = .6$, $\alpha_2 = .6$

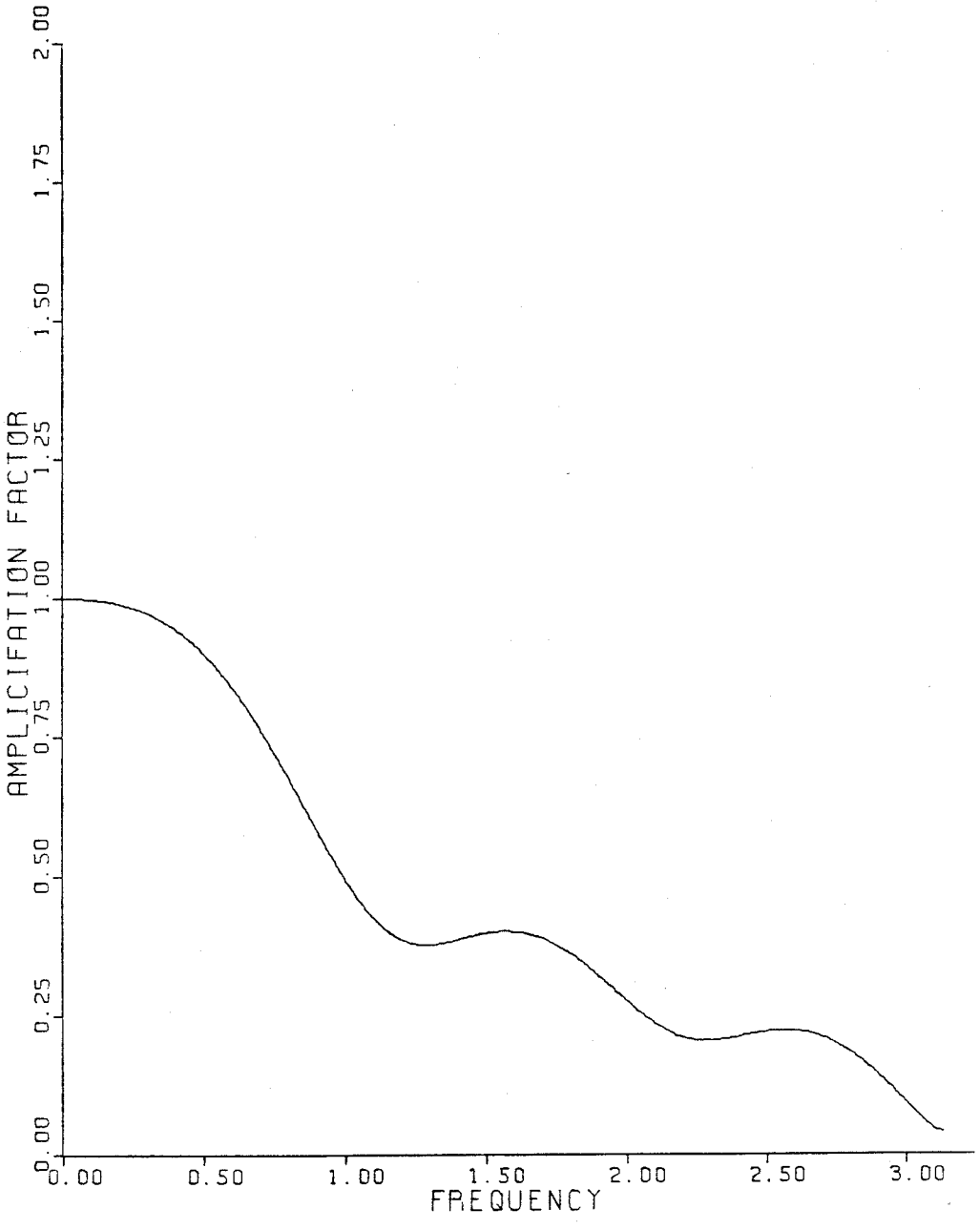

Figure 3(b)

Amplification factor $|g|$ of 3 stage scheme with single evaluation of dissipation for $\lambda = 1.5$, $\mu = .04$
Coefficients $\alpha_1 = .6$, $\alpha_2 = .6$

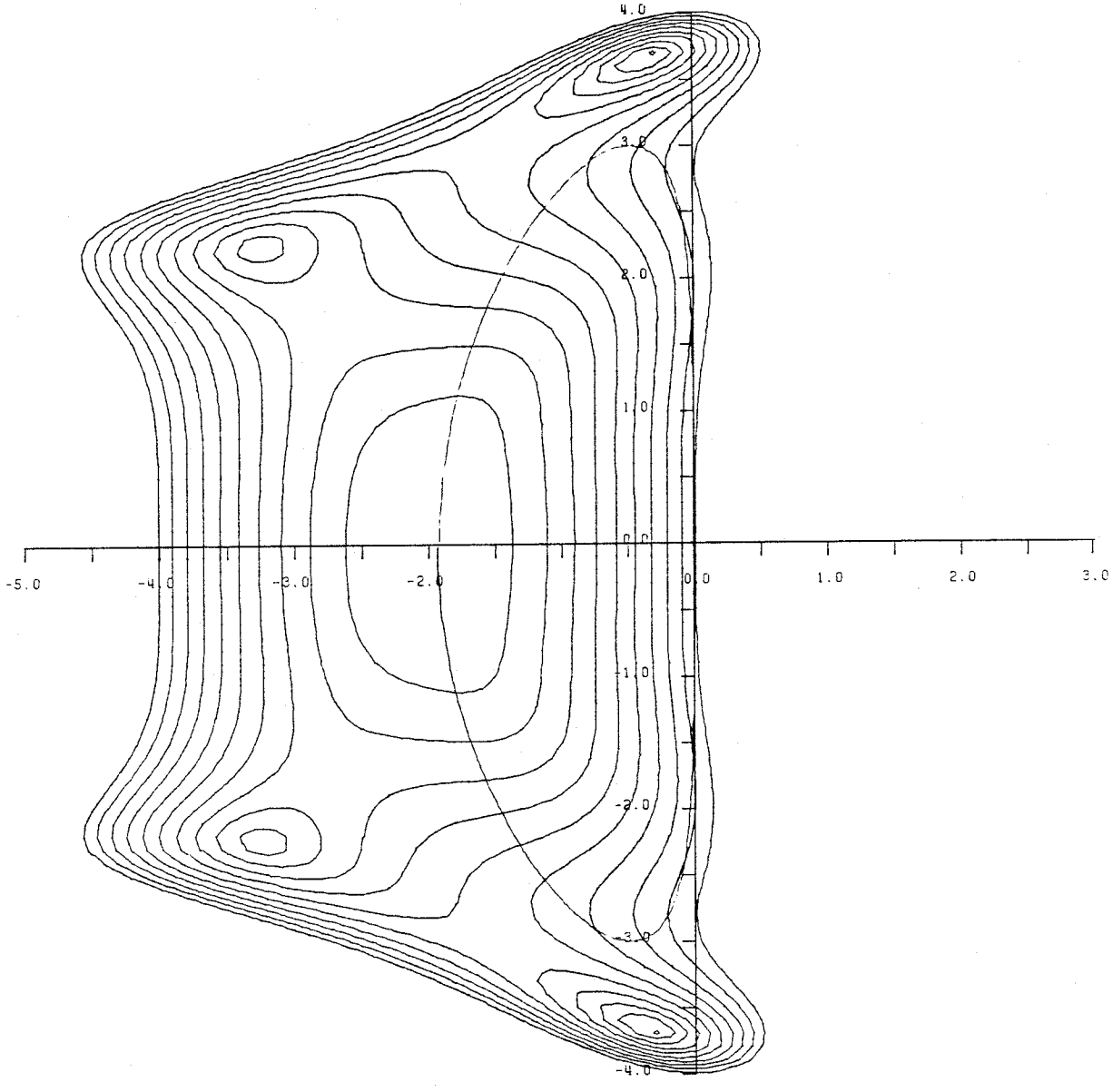

Figure 4(a)

Stability region of 5 stage scheme with two evaluations of dissipation
Contour lines $|g| = .9, .8, .7, \ldots$
and locus of $z(\xi)$ for $\lambda = 3.$, $\mu = .04$
Coefficients $\alpha_1 = 1/4$, $\alpha_2 = 1/6$, $\alpha_3 = 3/8$, $\alpha_4 = 1/2$, $\beta = 1$

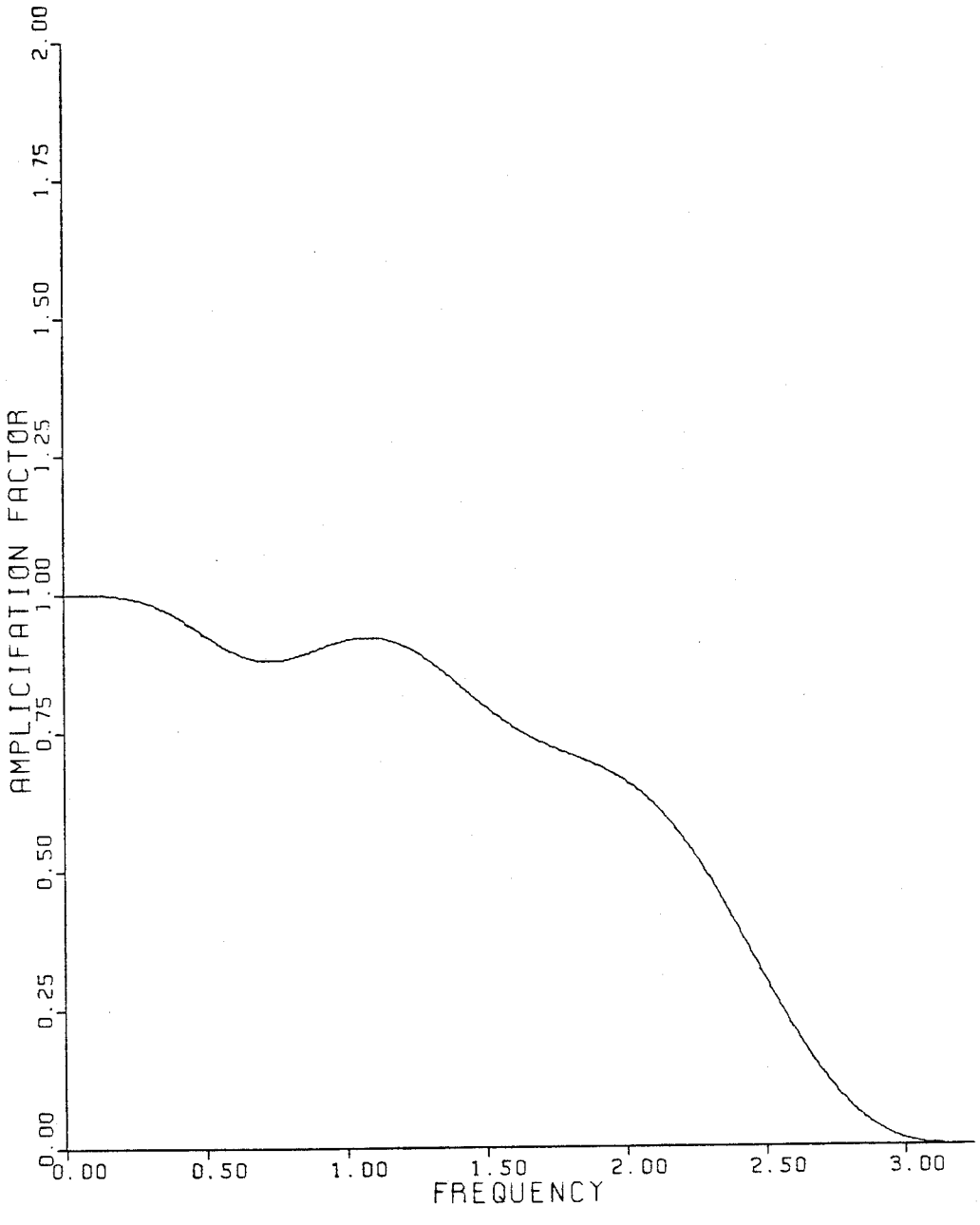

Figure 4(b)

Amplification factor $|g|$ of 5 stage scheme with
with two evaluations of dissipation
for $\lambda = 3$, $\mu = .04$
Coefficients $\alpha_1 = 1/4$, $\alpha_2 = 1/6$, $\alpha_3 = 3/8$, $\alpha_4 = 1/2$, $\beta = 1$

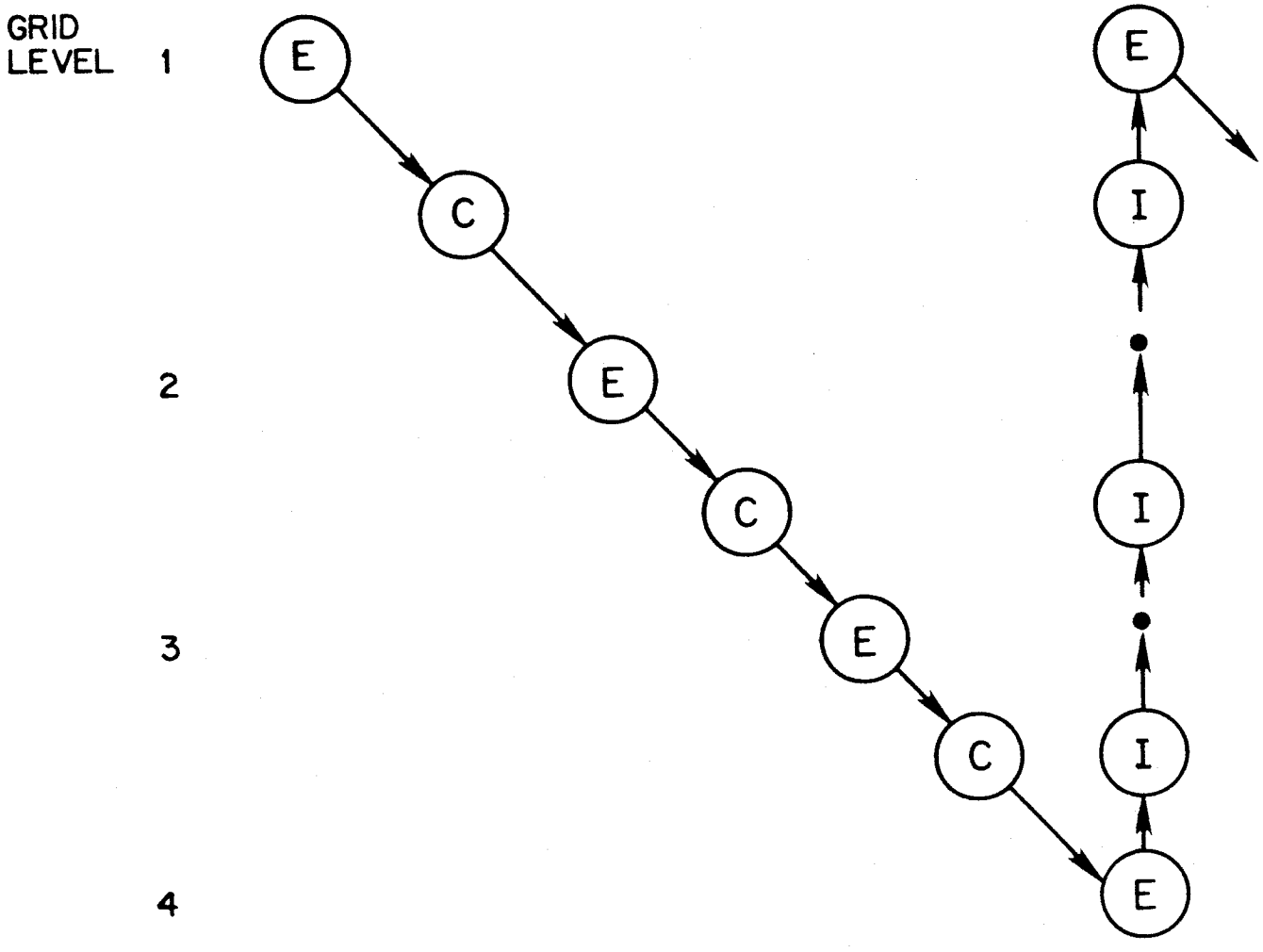

Figure 5

Saw Tooth Multigrid Cycle

(E) Euler Calculation

(C) Residual Calculation

(I) Interpolation

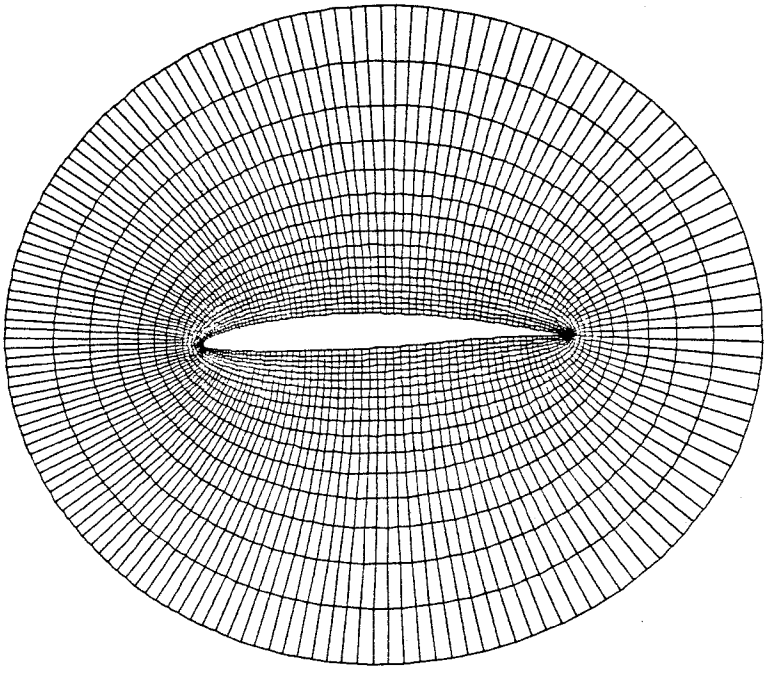

Figure 6(a)

Inner part of grid for NACA 64A410
160 x 32 cells

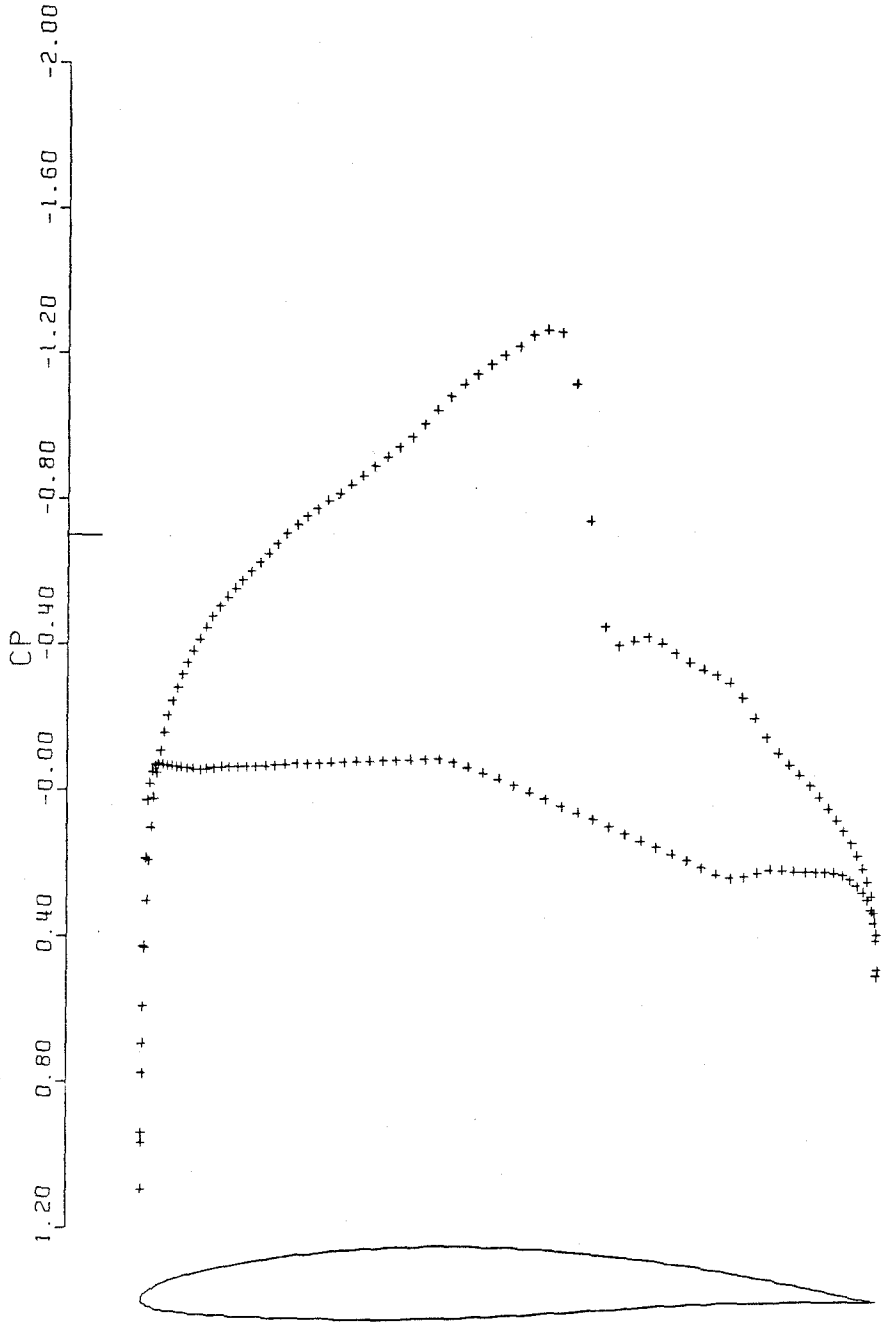

Figure 6(b)

Pressure distribution for NACA 64A410
Mach .720 α 0o
CL .6283 CD .0035
160 x 32 25 cycles Residual .539 10^{-3}

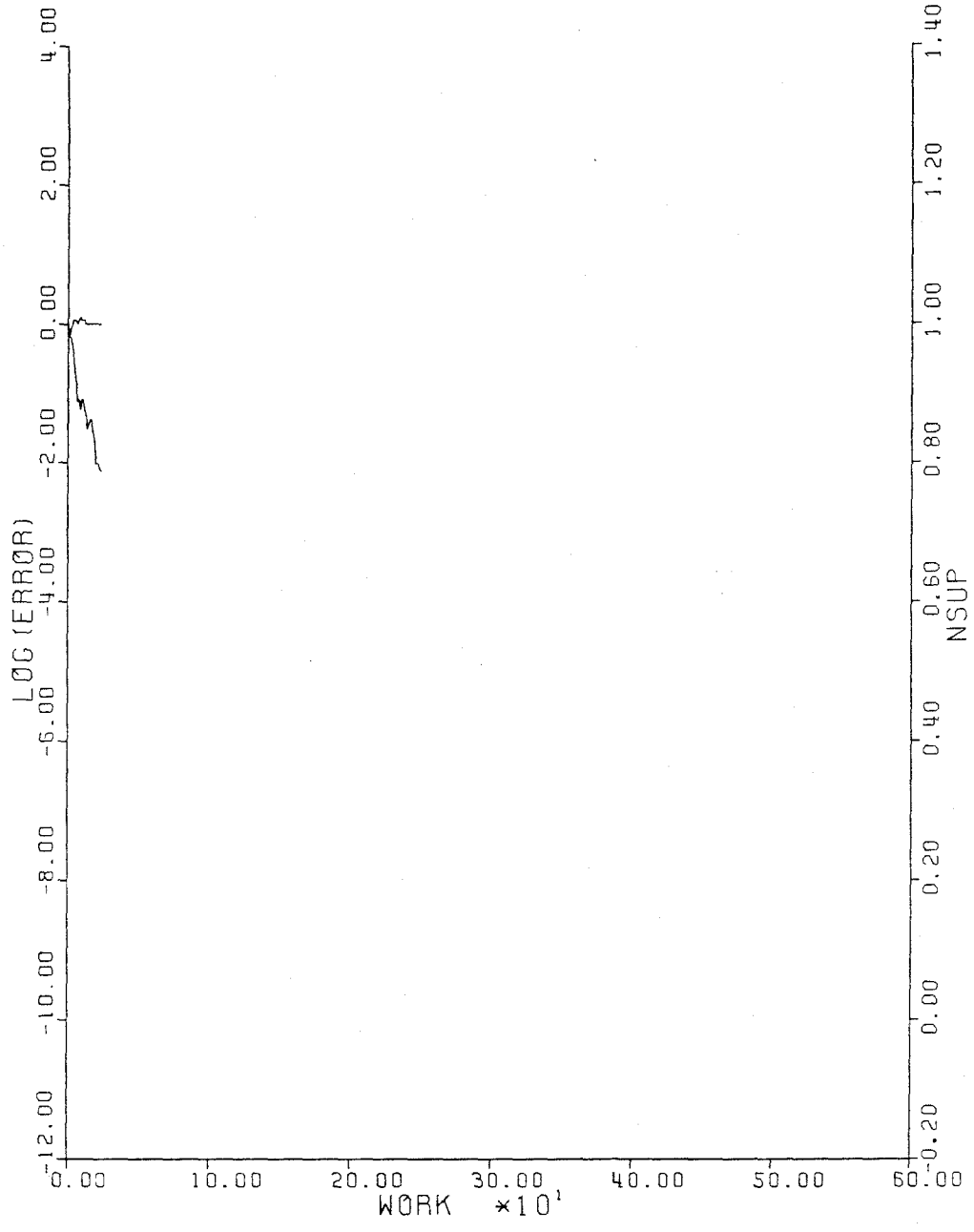

Figure 6(c)

Convergence history for NACA 64A410
Mach .720 α 0°
160 x 32 grid 25 cycles Residual .539 10^{-3}
Mean rate of convergence .8159 per cycle

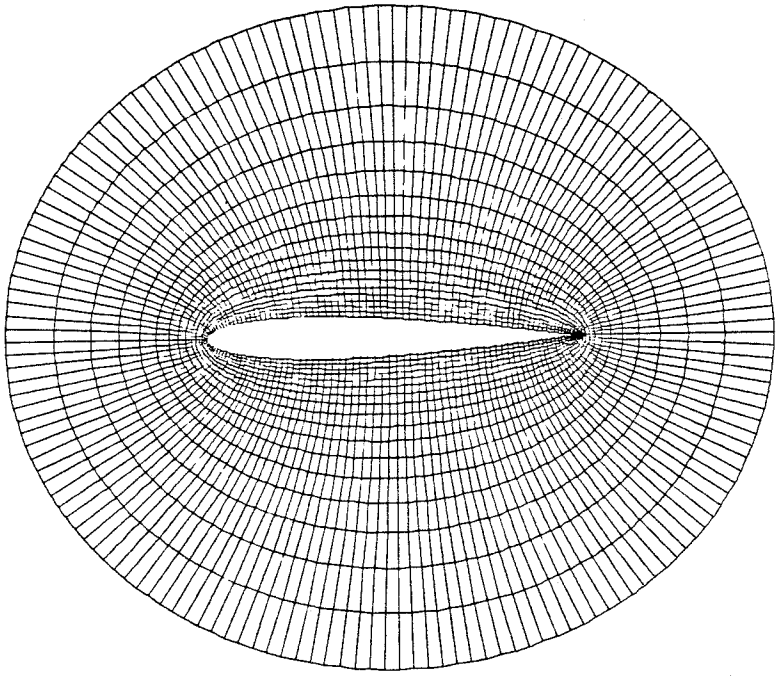

Figure 7(a)

Inner part of grid for NACA 0012
160 x 32 cells

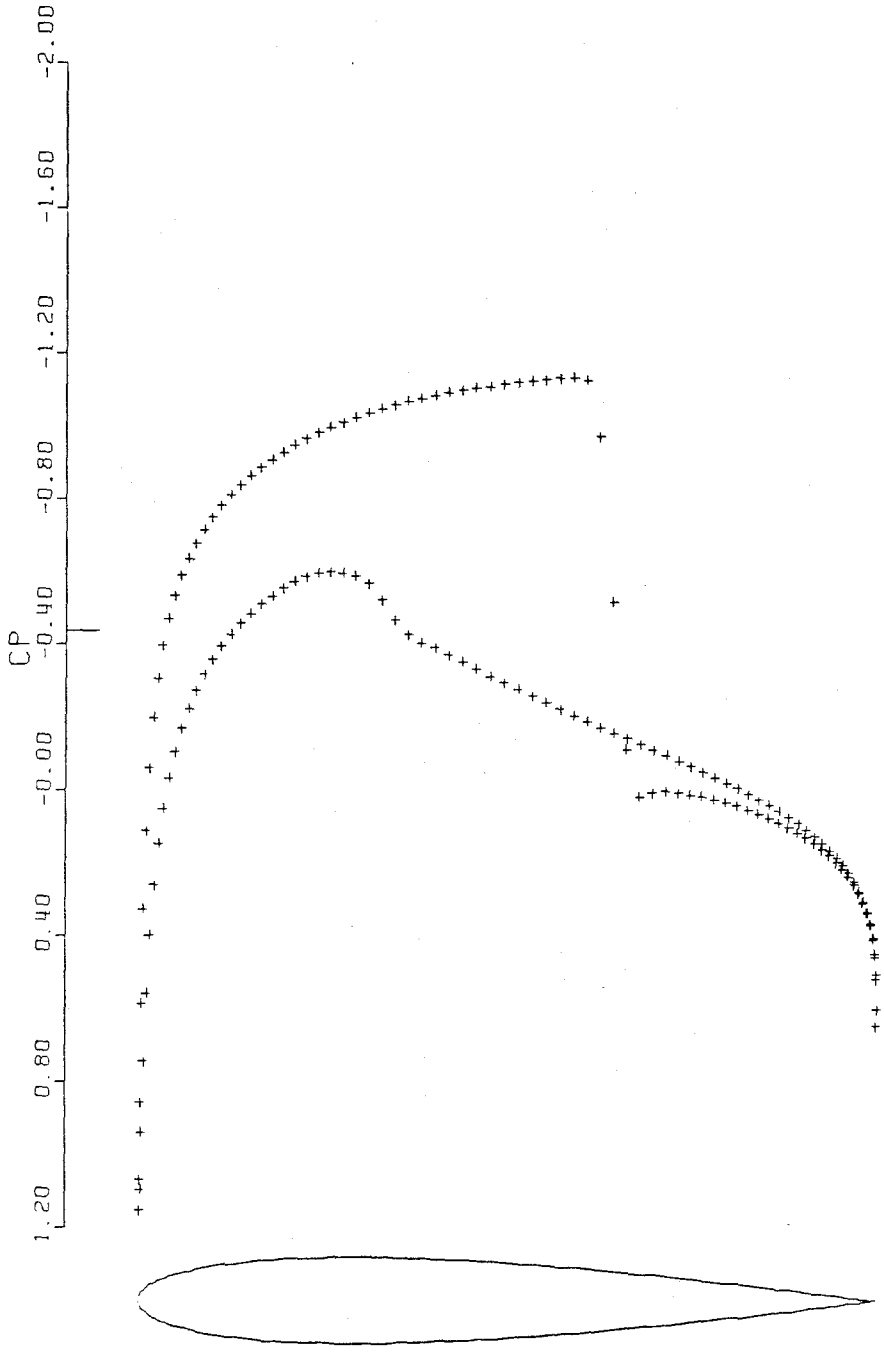

Figure 7(b)

Pressure distribution for NACA 0012
Mach .800 α 1.25°
CL .3615 CD .0233
160 x 32 grid 100 cycles Residual .655 10-4

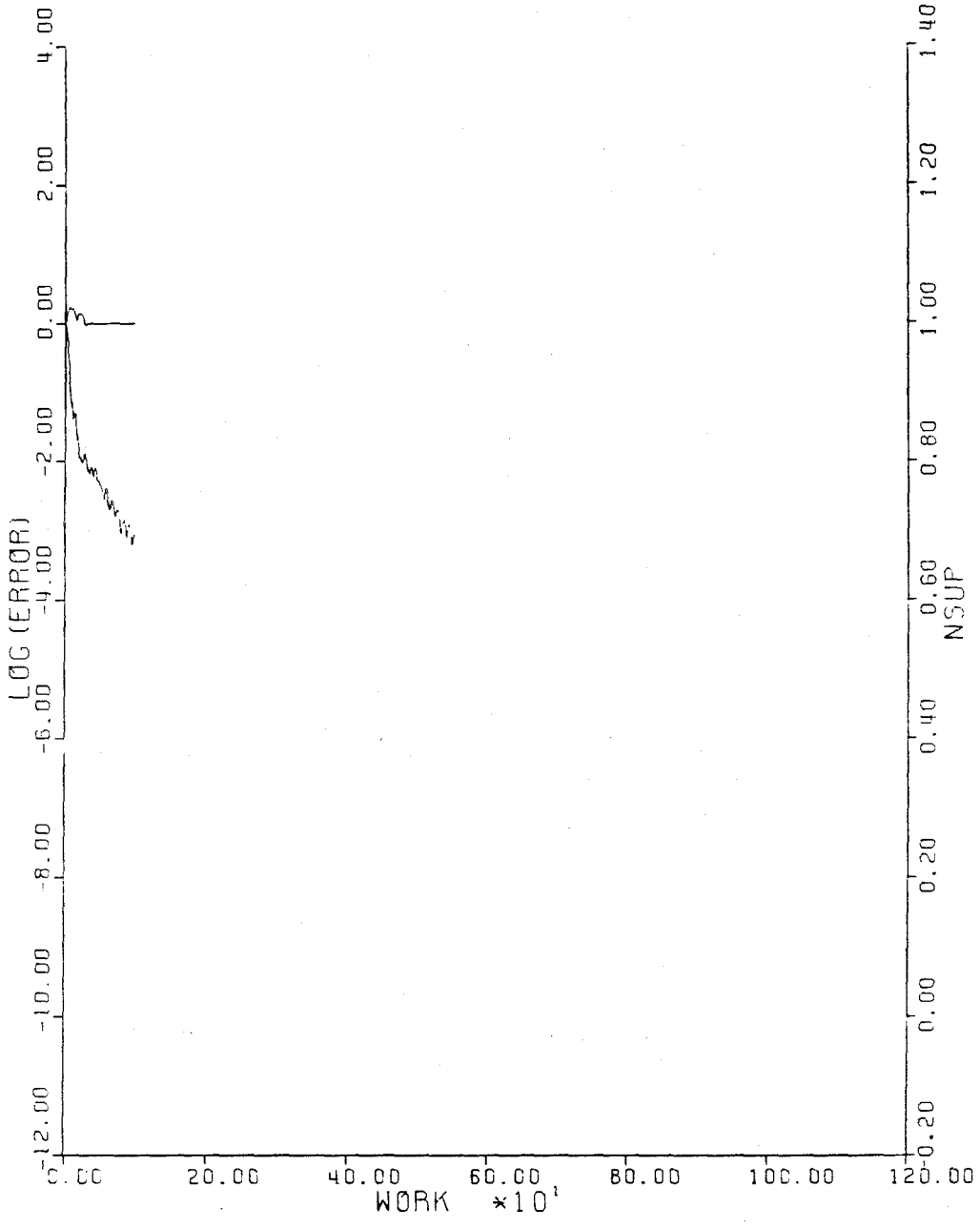

Figure 7(c)
Convergence history for NACA 0012
Mach .800 α 1.25°
160 x 32 100 cycles Residual .655 10^{-4}
Mean rate of convergence .9312 per cycle